Surface Science 606 (2012) 924–927

Contents lists available at SciVerse ScienceDirect

Surface Science

journal homepage: www.elsevier.com/locate/susc

Cobalt induced nanocrystals on Ge(001)

T.F. Mocking, G. Hlawacek, H.J.W. Zandvliet *

Physics of Interfaces and Nanomaterials, MESA+ Institute for Nanotechnology, University of Twente, P. O. Box 217, 7500 AE Enschede, The Netherlands

ARTICLE INFO

Article history:
Received 5 January 2012
Accepted 8 February 2012
Available online 21 February 2012

Keywords:
Cobalt
Nanocrystals
Shape transition
Germanium
Surface stress
STM
Helium Ion Microscopy

ABSTRACT

The deposition of several monolayers of cobalt on germanium (001) substrates results in the formation of two types of clusters: flat-topped and peaked nanocrystals. Scanning tunneling spectroscopy and helium ion microscopy measurements reveal that these nanocrystals contain cobalt. The shape evolution of the flat-topped and peaked nanocrystals as a function of their size is investigated with scanning tunneling microscopy. For small sizes the nanocrystals are compact. Beyond a critical size, however, the peaked nanocrystals exhibit an elongated shape, whilst the flat-topped nanocrystals remain compact. The shape transition of the peaked nanocrystals is driven by a competition between boundary and strain energies. For small sizes the boundary energy is the dominant term leading to a minimization of the peaked nanocrystal's perimeter, whereas at larger sizes the strain energy wins resulting in a maximization of the perimeter. On the top facet of the flat-topped nanocrystals one-dimensional structures are observed that are comprised of small square shaped units of about 1 nm^2. Time-resolved scanning tunneling microscopy measurements reveal that these square shaped units are dynamic at room temperature.

1. Introduction

The creation of low-dimensional and nanometer sized artificial structures on surfaces has been an important research topic for many decades. The interest in these nanostructures is huge because they exhibit attractive, and even more important, tunable electronic properties which pave the way to technologically relevant applications. The most straightforward way to tune the electronic properties of these nanostructures is by tailoring their size, shape and dimension. A way to accomplish control over these key parameters is to use the lattice misfit between substrate and nanostructure. Recent studies have revealed that the deposition of metals such as Pt [1], Au [2–4], and Co on semiconductor group IV (001) surfaces [5–14] leads to a plethora of novel nanostructures.

Several groups have studied the growth of Co on Si surfaces [15–20], while the growth of Co on Ge surfaces attracted much less attention. The growth of thicker Co layers on Ge(001) has, however, been addressed in quite some detail by Choi et al. [21] and De Keyser et al. [22]. In these studies several cobalt germanides, namely CoGe, $CoGe_2$ and Co_5Ge_7, were found. Ge and Si both have a diamond lattice with lattice constants of 0.566 nm and 0.543 nm, respectively. It is noteworthy to point out that the (001) projected lattice constant of Ge (0.40 nm) is very comparable to the c-lattice constant (0.407 nm) of the *hcp* Co lattice.

The lattice misfit in heteroepitaxial systems often leads to the formation of strain stabilized nanoclusters. In the early nineties of the twentieth century Tersoff and Tromp [23] put forward a generic model to explain the shape evolution of nanoclusters. They showed that strained islands are compact at small sizes, but become elongated beyond a certain critical size. An experimental study of the Co/Si(001) system by Brongersma et al. [20] revealed that this system almost perfectly obeys the generic Tersoff and Tromp model. The question that immediately pops up is whether the Co/Ge(001) system behaves in a similar fashion. This is a very relevant question, because both systems, i.e. Co/Si(001) and Co/Ge(001), behave differently at sub-monolayer Co coverages [5,15–20].

In this paper we will focus on the growth behavior of Co-induced nanocrystals on the Ge(001) surface. We have found a coexistence of peaked nanocrystals (PNCs) and flat-topped nanocrystals (FNCs). Scanning tunneling spectroscopy and helium ion microscopy measurements reveal that the chemical composition and structure of the PNCs and FNCs are significantly different from the underlying Ge substrate. Interestingly, only the PNCs exhibit a compact to elongated shape transition. On top of the FNCs one-dimensional structures are observed which show dynamic behavior at room temperature.

Experiments were performed with an Omicron ultra-high vacuum scanning tunneling microscope. The base pressure was $5 \cdot 10^{-11}$ mbar. Ge substrates were cut from nominally flat 3 in. single-side-polished and lightly Sb doped *n*-type wafers with a resistivity of less than 0.01 $\Omega \cdot$ cm. The samples were mounted on Mo holders and contact with any metal was avoided during the preparation. An atomically clean Ge(001) substrate was obtained by prolonged 800 eV Ar ion sputtering followed by annealing the sample through resistive heating at

* Corresponding author.
E-mail address: h.j.w.zandvliet@utwente.nl (H.J.W. Zandvliet).

0039-6028/$ – see front matter © 2012 Elsevier B.V. All rights reserved.
doi:10.1016/j.susc.2012.02.007

1100 (±25) K [24,25]. Several monolayers (3–5 monolayers) of Co were evaporated by resistively heating a W wire wrapped with a pure Co (99.995%) wire. The amount of deposited Co was kept constant throughout all our experiments. During evaporation the sample was kept at room temperature. After evaporation the sample was annealed at 600 (±25) K for 8 minutes and for a shorter period of 4 minutes at 700 (±25) K. Before placing it into the STM the sample was cooled down to room temperature. All STM measurements were performed at room temperature. Helium Ion Microscopy (HIM) [26] has been performed ex-situ after the STM investigations were completed. HIM images were recorded using both the Everhart–Thornley (ET) detector and the Micro Channel Plate (MCP) detector. While the first one allows the surface sensitive high resolution imaging of the sample morphology utilizing secondary electrons, the latter counts the number of back scattered helium atoms, thus allowing elemental and structural characterization of the specimen. Sample transfer from the UHV STM to the UHV HIM has been performed as quickly as possible. However, oxidation of both the Ge substrate and the Co nanocrystals during sample transfer cannot be excluded. The unique UHV-HIM [27] with a base pressure of $5 \cdot 10^{-9}$ mbar allows the prolonged exposure of the sensitive nanostructures to the helium beam. The primary energy of the He beam has been varied from 10 kV to 35 kV.

In Fig. 1(A) a room temperature scanning tunneling microscopy image of a Co/Ge(001) substrate is shown after the deposition of about 3 monolayers of Co and subsequent annealing at 600 K for 8 minutes and at 700 K for 4 minutes. The observed three-dimensional clusters can be divided into two different classes: (1) FNCs (Fig. 1(B)) and (2) PNCs (Fig. 1(C)). The PNCs can be divided into compact and elongated crystals. The PNCs have widths of about 10–35 nm and lengths of 10–60 nm. The FNCs have sizes ranging from about 20×20 nm^2 to 50×50 nm^2. The height of the nanocrystals varies between 4 nm and 7 nm. There is no firm relation between the surface projected size and the height of the PNCs and FNCs. The PNCs and the FNCs are always aligned along the high symmetry directions, i.e. the dimer row directions, of the (001) surface. The top of the FNCs is reconstructed. On top of these nanocrystals well-aligned one-dimensional structures are observed. The spacing between adjacent lines is often 2.8 ± 0.2 nm, but occasionally larger spacings of 3.2 ± 0.2 nm and 3.6 ± 0.2 nm are found as well. The one-dimensional structures or lines are composed of regularly spaced entities.

Scanning tunneling spectroscopy measurements are performed on the flat terraces as well as on the two types of nanocrystals. The differential conductivity, which is roughly proportional to the density of states, of the three different structures is shown in Fig. 2. The flat terraces display a rather large band gap which is comparable with the band gap of germanium. The differential conductivities of the two types of nanocrystals are distinctly different, but both exhibit a clear metallic character. Since the density of states of the nanocrystals is so different from that of Ge we have to conclude that both types of nanocrystals contain Co. The crystal structure and exact chemical composition of both types of nanocrystals are probably different as well. Possible candidates for the nanocrystals are $CoGe_2$, Co_5Ge_7 or CoGe [20,21]. The distinct peak in the density of states observed for FNCs at −0.5 V bias voltage is a typical fingerprint of Co [28,29]. This indicates that the flat top facet of the FNCs consists of Co atoms.

HIM has been used to check the homogeneity of the sample surface. In the 1 μm² large ET HIM image presented in Fig. 3(A) a total of roughly 250 nanocrystals can be seen. The average aspect ratio (AR) is 1.54. However, the presence of the elongated nanocrystals leads to a second maximum in the distribution at an AR of 1.70 and a maximum AR of 3.13. The comparable low energy of the secondary electrons – created by the energy loss of the He due to electronic stopping in the material – and their origin from a surface near region make the method very sensitive to changes of the work function. The contrast between the nanocrystals and the germanium substrate is based on this effect. The back scattered helium image presented in Fig. 3(B) has been obtained using the MCP detector. The nanocrystals are clearly visible and also their different shapes can be identified. Here contrast is based on the backscatter probability of He. However, for this particular sample the contrast stems not from the different backscatter probabilities of cobalt and germanium. Depending on the thickness of the lighter Co top-layer either no contrast (thin Co film) or a reverse contrast (thick Co layer) would be expected. The increased backscatter probability is a result of the different crystal structures of the nanocrystals. The incommensurate nanocrystals block the open channels in the underlying Ge(001) substrate, thus locally increasing the backscatter yield. This is confirmed by Fig. 3(C), which has been recorded under identical conditions but with a 10°

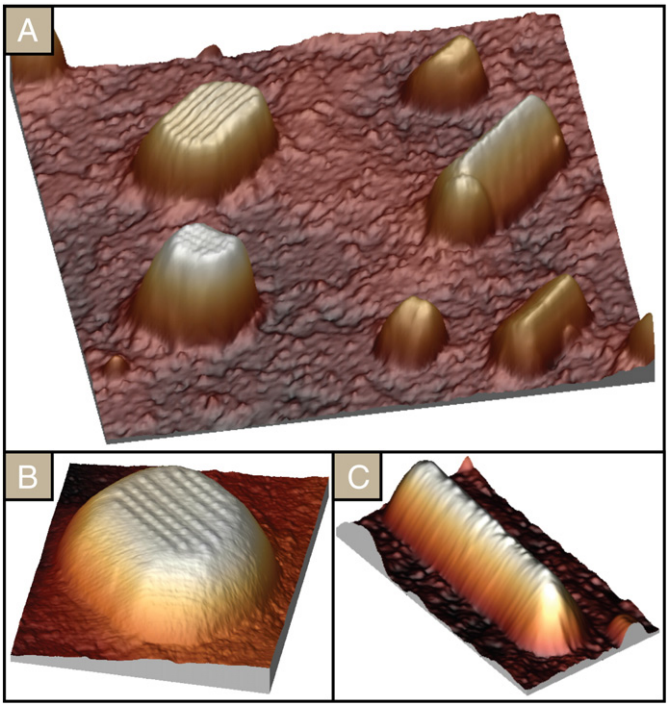

Fig. 1. Scanning tunneling microscopy images of Co induced nanocrystals on a Ge(001) substrate. (A) An overview on the Co-induced nanocrystals on the Ge(001) surface. The image size is 140×140 nm^2. The height of the highest nanocrystal is 6 nm. Two different types of crystals are observed: (B) flat-topped nanocrystals (FNCs) and (C) peaked nanocrystals (PNCs). Images (B) and (C) have sizes of 50×50 nm^2 and 30×55 nm^2, respectively. Sample bias is −1.5 V and tunneling current is 0.5 nA. The heights of the nanocrystals in (B) and (C) are 6 nm and 5 nm, respectively.

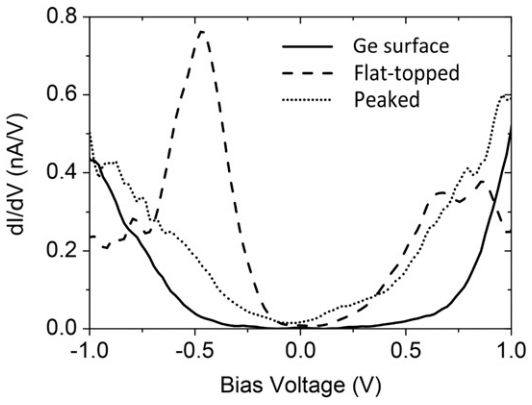

Fig. 2. Differential conductivity (dI/dV) recorded on bare Ge(001) terraces (solid line), flat-topped nanocrystals (large dash) and peaked nanocrystals (small dash). The results are averaged over more than 100 traces per curve, with setpoints $I_t = 0.45$ nA and $V_g = -1.5$ V.

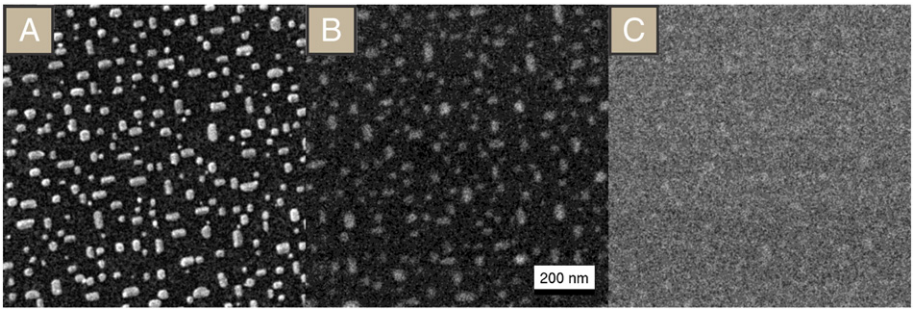

Fig. 3. (A) Everhart–Thornley He ion microscope image (FOV: 1 μm²) obtained at 35 kV with a beam current of 0.2 pA and a dwell time of 80 μs. About 250 PNCs and FNCs are visible. (B) Back scattered He image (1 μm²) of the same sample recorded with 10 kV, a beam current of 0.1 pA and a dwell time of 160 μs. PNCs and FNCs are visible as they locally increase backscatter probability by lifting the channeling condition for the underlying Ge(001) crystal. (C) Back scattered He image recorded under identical conditions as (B) but with a sample tilt of 10°. Under this non channeling condition for the Ge(001) wafer the nanostructures cannot be seen.

sample tilt. The (001) channels are not parallel to the He ion beam anymore and backscattering has increased on the whole sample surface rendering the nanocrystals invisible.

The width and length (w and l, respectively) of the PNCs and FNCs are plotted against the square root of the island size in Fig. 4. Beyond a critical island size of about 400 nm^2 a shape transition from compact PNC to elongated PNC is observed. Brongersma et al. [20] have found a similar shape transition of $CoSi_2$ clusters on Si(001). However, in the Co/Si(001) case the shape transition occurred at a much larger cluster size [20]. The FNCs, which turn out to be always larger than 400 nm^2, remain compact up to at least 2000 nm^2. A possible explanation for the latter is that the critical crystal size is simply larger than 2000 nm^2, but it might also be that these FNCs do not exhibit this shape transition at all i.e. the FNCs could already be relaxed by misfit dislocations. This way they do not require sharp apexes and shape transitions to relax the strain [13,14]. Interestingly, we did not observe even a single FNC that has a size smaller than the critical PNC size, suggesting that PNCs with the critical size can evolve in either elongated PNCs or compact FNCs.

The shape of nanostructures on surfaces is in general governed by two energetic terms, the boundary energy and strain relaxation energy. The boundary energy term favors compact nanostructure shapes, whereas the strain relaxation term prefers to maximize the total boundary length. As pointed out by Tersoff and Tromp [23] a balance of these two terms reveals that nanostructures on surfaces, i.e. islands or nanoclusters, are compact for small sizes and elongated for large sizes. The latter is of course true for heteroepitaxial systems where a lattice misfit is virtually always present; however Li et al. [30] and Zandvliet et al. [31] have shown that it can also hold for homoepitaxial systems.

A topography image of the one-dimensional structures on top of the FNCs is displayed in Fig. 5(A). In Fig. 5(A) several of these wires are shown and a profile scan has been made along the arrow. The profile scan is depicted in Fig. 5(B). The wires are positioned at least 2.8 ± 0.2 nm apart, but larger distances, i.e. 3.2 ± 0.2 nm and 3.6 ± 0.2 nm are sometimes observed as well. The wires are comprised of small square-shaped features that have a size of about 1 nm^2. The height of these entities is 0.14 ± 0.02 nm. Furthermore, the square-shaped entities have a preferred nearest neighbor intrarow spacing of 1.6 ± 0.2 nm; however smaller and larger distances do occasionally occur. The ordering of the entities in neighboring rows is in virtually all cases out of phase. Some of the square-shaped entities have a frizzy

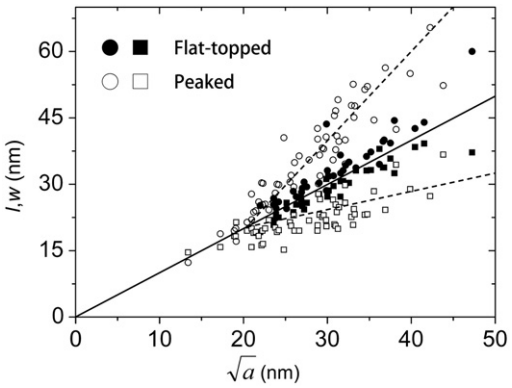

Fig. 4. Length 'l' (circles) and width 'w' (squares) of the FNCs and PNCs as a function of the square root of the projected surface area of the PNCs or FNCs. PNCs with a projected surface area larger than about 400 nm^2 have an elongated shape, whereas smaller PNCs are compact. FNCs are compact for sizes up to at least 2000 nm^2.

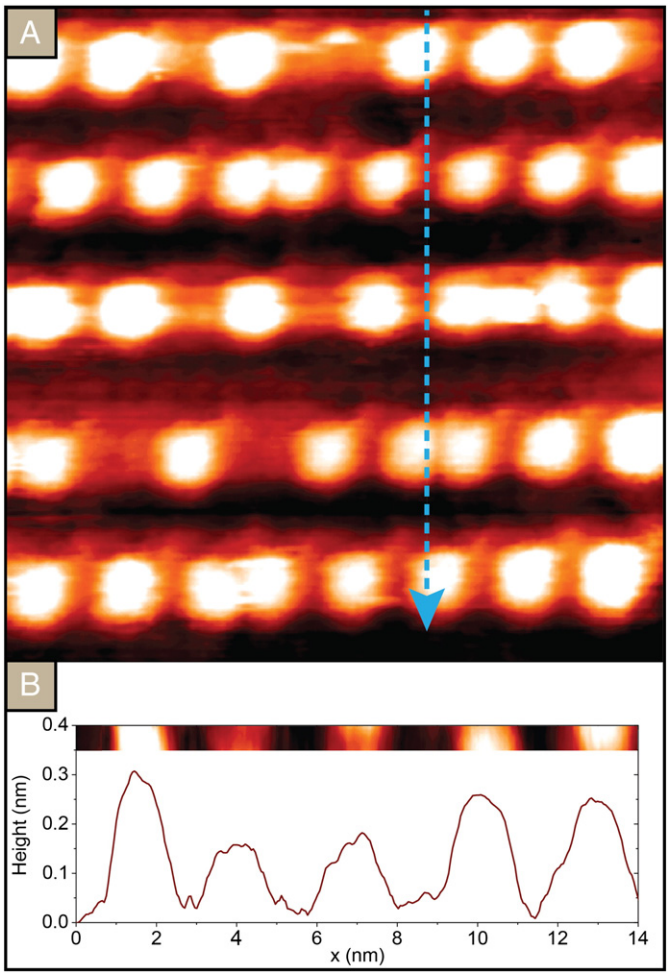

Fig. 5. (A) A close-up of the one-dimensional structures observed on top of the FNCs. (B) A line scan taken along the arrow. Sample bias is +1.5 V and tunneling current is 0.6 nA.

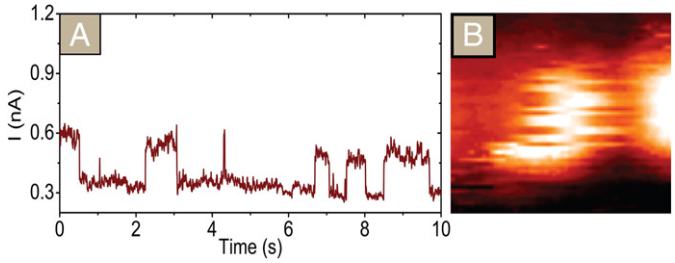

Fig. 6. (A) A current time trace with the feedback loop disabled taken on one of the dynamic entities of the one-dimensional structures which are observed on the FNCs. Two distinct levels are observed indicating that the entity hops back and forth between two positions. (B) STM image (4 nm^2) of a dynamic entity that jumps back and forth between two positions (the image is scanned from bottom to top and from left to right). Sample bias is +1.5 V and tunneling current is 0.6 nA.

appearance in the scanning tunneling microscopy images. For instance, the entity in the middle of the topmost row jumps from left to right (the image is scanned from bottom to top and from left to right). It should be noted that this entity was not present in the first few scan lines of this row. The latter implies that the entity has diffused to this row during imaging.

These dynamic entities are observed quite frequently and a nice example is given in Fig. 6. The frizzy appearance of the entity indicates that it jumps back and forth between two positions. Current–time traces with the feedback loop disabled are taken on top of the entity shown in Fig. 6(B). An example of such a current–time trace is depicted in Fig. 6(A). Two current levels can be distinguished and within 10 seconds the entity jumps back and forth several times. The typical jump frequency of the square-shaped entity is about 1 Hz. The averaged jump frequency is independent of the actual sample bias and tunneling current set points indicating that the observed motion is thermally induced. The majority of the jumps occur within the chain. Similar observations have been made for Si on Si(111)-(5x2)-Au [32]. Interestingly, there are a few more analogies between these two systems: (1) the well-defined spacing between adjacent chains, (2) the well-defined spacing between entities within the chain and (3) the out-of-phase registry of the entities within adjacent chains.

The size and height of the square shaped units suggest that they are comprised of two Ge dimers. In addition, imaging at +1.5 V and −1.5 V sample bias results in very similar appearing images, which is another hallmark of Ge dimers. However, our measurements are not conclusive regarding the exact structure and composition of these square shaped units. In particular, the STS data recorded on top of the FNCs reveal a clear signature of Co.

In summary, the deposition of Co on Ge(001) and subsequent annealing leads to the formation of two types of nanoclusters, namely PNCs and FNCs. Scanning tunneling spectroscopy and He ion microscopy measurements reveal that the nanocrystals contain cobalt. The PNCs are compact below a critical island size of about 400 nm^2 and elongated beyond that size. The FNCs are, however, compact up to at least 2000 nm^2. On the top facet of these FNCs one-dimensional structures are found. These one-dimensional structures are perfectly straight, have a height of two atomic layers and the top layer consists of square-shaped entities. Some of these entities exhibit dynamic motion during imaging.

Acknowledgments

This research is supported by the Dutch Technology Foundation STW, which is the applied science division of NWO, and the Technology Programme of the Ministry of Economic Affairs.

References

[1] O. Gurlu, O.A.O. Adam, H.J.W. Zandvliet, B. Poelsema, Appl. Phys. Lett. 83 (2003) 4610.
[2] J. Wang, M. Li, E.I. Altman, Phys. Rev. B 70 (2004) 233312.
[3] J. Schäfer, C. Blumenstein, S. Meyer, M. Wisniewski, R. Claessen, Phys. Rev. Lett. 101 (2008) 236802.
[4] K. Nakatsuji, R. Niikura, Y. Shibata, M. Yamada, T. Iimori, F. Komori, Phys. Rev. B 80 (2009) 081406.
[5] H.J.W. Zandvliet, A. van Houselt, P.E. Hegeman, Surf. Sci. 605 (2011) 1129.
[6] I. Goldfarb, G.A.D. Briggs, J. Mater. Res. 16 (2001) 744.
[7] I. Goldfarb, G.A.D. Briggs, J. Vac. Sci. Technol. B 20 (2002) 1419.
[8] H.P. Sun, Y.B. Chen, X.Q. Pan, D.Z. Chi, R. Nath, Y.L. Foo, Appl. Phys. Lett. 87 (2005) 211909.
[9] H.P. Sun, Y.B. Chen, X.Q. Pan, D.Z. Chi, R. Nath, Y.L. Foo, Appl. Phys. Lett. 86 (2005) 071904.
[10] A. Tsuruta, W.G. Chu, K. Tamura, H. Ishii, M. Owari, Y. Nihei, Surf. Interface Anal. 37 (2005) 230.
[11] S. Gaudet, C. Detavernier, A.J. Kellock, P. Desjardins, C. Lavoie, J. Vac. Sci. Technol. A 24 (2006) 474.
[12] V.G. Mygkov, Y.L. Mikhlin, L.E. Bykova, G.N. Bondarenko, I.A. Turpanov, Doklady Phys. Chem. 431 (2010) 72.
[13] I. Goldfarb, Surf. Sci. 601 (2006) 2756.
[14] I. Goldfarb, G. Cohen-Taguri, S. Grossman, M. Levinshtein, Phys. Rev. B 72 (2005) 075430.
[15] I. Goldfarb, S. Grossman, G. Cohen-Taguri, Appl. Surf. Sci. 252 (2006) 5355.
[16] I. Goldfarb, G.A.D. Briggs, Phys. Rev. B 60 (1999) 4800.
[17] I. Goldfarb, L. Banks-Sills, R. Eliasi, Interface Sci. 10 (2002) 75.
[18] V. Scheuch, B. Voigtländer, H.P. Bonzel, Surf. Sci. 372 (1997) 71.
[19] S.H. Brongersma, M.R. Castell, D.D. Perovic, M. Zinke-Allmang, J. Vac. Sci. Technol. B 16 (1998) 2188.
[20] S.H. Brongersma, M.R. Castell, D.D. Perovic, M. Zinke-Allmang, Phys. Rev. Lett. 80 (1998) 3795.
[21] J. Choi, D.K. Lim, Y. Kim, S. Kim, J. Phys. Chem. C 114 (2010) 8992.
[22] K. De Keyser, R.L. Van Meirhaeghe, C. Detavernier, J. Jordan-Sweet, C. Lavoie, J. Electrochem. Soc. 157 (2010) H395.
[23] J. Tersoff, R.M. Tromp, Phys. Rev. Lett. 70 (1993) 2782.
[24] H.J.W. Zandvliet, B.S. Swartzentruber, W. Wulfhekel, B.J. Hattink, B. Poelsema, Phys. Rev. B 57 (1998) 6803.
[25] H.J.W. Zandvliet, Phys. Rep. 388 (2003) 1.
[26] R. Hill, F.H.M. Faridur Rahman, Nucl. Instrum. Methods Phys. Res. A 645 (2011) 96.
[27] R. van Gastel, L. Barriss, C. Stanford, G. Hlawacek, L. Scipioni, A.P. Merkle, D. Voci, C. Fenner, H.J.W. Zandvliet, B. Poelsema, Microsc. Microanal. 17 (S2) (2011) 928.
[28] D. Eom, D. Prezzi, K.T. Rim, H. Zhou, M. Lefenfeld, S. Xiao, C. Nuckolls, M.S. Hybertsen, T.F. Heinz, G.W. Flynn, Nanoletters 9 (2009) 8.
[29] M.A. Barral, M. Weissmann, A.M. Llois, Phys. Rev. B 72 (2005) 125433.
[30] A. Li, F. Liu, M.G. Lagally, Phys. Rev. Lett. 85 (2000) 1922.
[31] H.J.W. Zandvliet, R. van Gastel, Phys. Rev. Lett. 99 (2007) 136103.
[32] E. Bussmann, S. Bockenhauer, F.J. Himpsel, B.S. Swartzentruber, Phys. Rev. Lett. 101 (2008) 266101.